

Realization of entanglement-assisted weak-value amplification in a photonic systemJiang-Shan Chen, Bi-Heng Liu,^{*} Meng-Jun Hu, Xiao-Min Hu, Chuan-Feng Li,
Guang-Can Guo, and Yong-Sheng Zhang[†]*CAS Key Laboratory of Quantum Information, University of Science and Technology of China, Hefei 230026, People's Republic of China
and CAS Center For Excellence in Quantum Information and Quantum Physics, University of Science and Technology of China,
Hefei 230026, People's Republic of China*

(Received 22 November 2018; published 25 March 2019)

Weak-value amplification has been used to enhance the sensitivity of a linear detector response to small interaction parameters. However, the generation of a large weak value gives rise to reduction in postselection probability, which restricts the feasibility of the weak-value amplification technique. Recently, theoretical works have shown that the use of entanglement can increase the efficiency of the weak-value amplification method. Specifically, it is proven that by entangling n particles of a system, the maximum postselection probability scales quadratically with n [Pang, Dressel, and Brun, *Phys. Rev. Lett.* **113**, 030401 (2014)]. In this work, we demonstrate an experimental realization of entanglement-assisted weak-value amplification in a photonic system, which shows that importing quantum entanglement can indeed improve the efficiency of weak-value amplification.

DOI: [10.1103/PhysRevA.99.032120](https://doi.org/10.1103/PhysRevA.99.032120)**I. INTRODUCTION**

Measurement is one of the most important foundations in physics. In quantum mechanics, it is deemed that any average of a measurement operator must range in the smallest and largest of its eigenvalues. Afterwards Aharonov, Albert, and Vaidman found the exceptions to this conclusion by introducing the concept of weak value [1]. They designed a Gedanken experiment to measure a spin-1/2 particle and obtain the average spin far beyond the eigenvalue range of the spin operator. Such an average spin, i.e., weak value, describes the mean effect of the postselected system ensemble that would largely shift the intercoupled pointer states designed to measure the target operator; hence, the weak value does not really reflect the measurement operator. Generally, in order to realize this effect, people must carry out the procedure as follows: (1) preparation of an initial quantum system state; (2) a weak interaction that couples an observable of the system with a variable of the meter; and (3) postselection on a final quantum system state.

Since weak values possess many interesting features that have been studied extensively both theoretically and experimentally [2–6], they serve as a powerful tool to explore fundamental questions in quantum mechanics [7–11]; in particular, they aid the discovery of many counterintuitive quantum results [12,13]. The peculiar feature of weak value leads to its active exploitation of quantum technology, for example, in the direct measurement of quantum states [14–17], and for its role in the methods that help resolve paradoxes, such as Hardy's paradox [12,18], and more general counterfactual quantum problems, such as the three-box problem [9,19].

The fact that a weak value can be far beyond the eigenvalue spectrum of measurement observable has led directly to an important applications of weak values, i.e., weak-value amplification [20,21], to improve the sensitivity of measurement. By this scheme, one can amplify the apparent strength of a signal in measurement, thus enabling the detection or measurement of tiny physical quantities that would be impractical to measure with traditional methods [22–30]. One dramatic achievement of weak-value amplification is the observation of the spin Hall effect of light demonstrated by Hosten and Kwiat [22]. Unfortunately, this sensitivity increase comes at the expense of a reduction in the sample size due to postselection. Thus, there is much controversy about the effectiveness of weak-value amplification acting as a parameter estimation technique [31–35], and some studies have shown that weak-value amplification may reduce the potential estimation precision and nullify any potential improvement in the signal-to-noise ratio (SNR) in most scenarios [33,36–41]. Despite these concerns, several theoretical and experimental works have shown that weak measurement can provide a practical advantage over conventional measurement when various kinds of noise are presented [22,24,27]. One further theoretical study has shown that weak-value amplification can surpass conventional measurement when detector saturation is coupled with intrinsic pixel noise and/or pixel digitization [42].

Recently, it has been shown by Pang *et al.* [43] that the utilization of entanglement can increase the efficiency of the weak-value amplification method. More specifically, it is demonstrated that by entangling n single-system states, the maximum postselection probability P_{\max} can be increased by a factor of n while keeping the weak value fixed compared to n uncorrelated attempts with a single system, i.e., P_{\max} can be increased by a factor of n^2 compared to one attempt with a single system. In this paper, we experimentally demonstrate

^{*}bhliu@ustc.edu.cn[†]yshzhang@ustc.edu.cn

entanglement-assisted weak-value amplification in a photonic system with genuine single photons. We show that by entangling two degrees of freedom of a system, the postselection probability can be increased approximately by a factor of 4 while keeping the weak value fixed (compared to one attempt with one single system), which shows that importing quantum entanglement can effectively increase the efficiency of weak-value amplification. Therefore, here, the essence of the quantum resources in our case is entanglement of two path qubits instead of entanglement of two photons, and there is no nonlocality for the entanglement. The results shown here also demonstrate the greater usefulness of entanglement, which can encourage further development in quantum measurement and metrology.

This paper is organized as follows. In Sec. II we give a brief review of the theory of entanglement-assisted weak-value amplification. In Sec. III, we illustrate the principle and proposal of our experiment. In Sec. IV, we show the results of our experiment. In Sec. V, we discuss and conclude our work.

II. REVIEW OF THEORY

In this section, we review the derivation of Pang *et al.* [43]. Later, we will adopt their notation in the derivation of the weak value for our experimental system, shown in the Appendixes. Pang *et al.* begin by defining an interaction Hamiltonian that couples the system to the pointer variable, and the interaction Hamiltonian of the form can be written as

$$\hat{H}_{\text{int}} = \hbar g \hat{A} \otimes \hat{F} \delta(t - t_0), \quad (1)$$

where \hat{A} is an observable of the system, \hat{F} is a meter observable, and g is the small coupling parameter that estimates the coupling strength of the system and meter. The time factor $\delta(t - t_0)$ manifests that the interaction is impulsive. Suppose that one prepares the system in a pure initial state $|\psi_i\rangle$, weakly couples it using the above interaction Hamiltonian, and then postselects the system into a pure final state $|\psi_f\rangle$. The weak value of observable \hat{A} is defined as $A_w = \langle \psi_f | \hat{A} | \psi_i \rangle / \langle \psi_f | \psi_i \rangle$ [1]. A large A_w can effectively amplify the small parameter g to be estimated. It also has the disadvantage of the low efficiency of weak-value amplification, since the postselection probability approximates $P_s \approx |\langle \psi_f | \psi_i \rangle|^2$, for small g .

Now consider an uncorrelated case that $\hat{A} = \hat{\sigma}_z$, in which the system is preselected in the state $|\psi_i\rangle = |+\rangle = \frac{1}{\sqrt{2}}(|0\rangle + |1\rangle)$ and postselected in the state $|\psi_f\rangle \propto (1 + \epsilon)|0\rangle - (1 - \epsilon)|1\rangle$, where ϵ should be considered to be relatively small. (This postselected state is different from the corresponding state shown in [43] which has used postselected state $|\psi_f\rangle = (e^{-i\epsilon}|0\rangle - e^{i\epsilon}|1\rangle)/\sqrt{2}$.) In this case, we can obtain the weak value of $A_w = \langle \psi_f | \hat{A} | \psi_i \rangle / \langle \psi_f | \psi_i \rangle = 1/\epsilon$ with an approximate probability $P_s \approx \epsilon^2$.

We then consider the correlated case in which the meter is coupled to n identical single-system observables with the interaction of Eq. (1). Such an operation couples the meter to a joint system observable,

$$\hat{A} = \hat{A}_1 + \dots + \hat{A}_n, \quad (2)$$

where $\hat{A}_k = \hat{I} \otimes \dots \otimes \hat{a} \otimes \dots \otimes \hat{I}$ is the shorthand for observable \hat{a} of the k th single system. If one prepares the entangled system

of n identical single systems in a joint state $|\psi_i\rangle$ and then postselects it in a joint state $|\psi_f\rangle$ to produce a joint weak-value amplification with the factor of A_w , there can be an optimal choice that maximizes the postselection probability, which can be realized by setting the preparation states and the postselection states as follows [43]:

$$\begin{aligned} |\psi_i\rangle &= \frac{1}{\sqrt{2}}(|\lambda_{\text{max}}\rangle^{\otimes n} + e^{i\theta}|\lambda_{\text{min}}\rangle^{\otimes n}), \\ |\psi_f\rangle &\propto -(n\lambda_{\text{min}} - A_w^*)|\lambda_{\text{max}}\rangle^{\otimes n} \\ &\quad + e^{i\theta}(n\lambda_{\text{max}} - A_w^*)|\lambda_{\text{min}}\rangle^{\otimes n}, \end{aligned} \quad (3)$$

where λ_{max} and λ_{min} are the maximum and the minimum eigenvalues of \hat{a} respectively, while $|\lambda_{\text{max}}\rangle$ and $|\lambda_{\text{min}}\rangle$ are the corresponding eigenstates, and θ is an arbitrary relative phase and here will be chosen as $\theta = 0$. Both the above forms explicitly depend on the chosen value of A_w . Furthermore we can verify that $\langle \psi_f | \hat{A} | \psi_i \rangle / \langle \psi_f | \psi_i \rangle = A_w$ and, in the case of $|A_w| \gg n\lambda_{\text{max}}$, $|\langle \psi_f | \psi_i \rangle|^2 \approx n^2(\lambda_{\text{max}} - \lambda_{\text{min}})^2/4|A_w|^2$, which shows that introducing quantum entanglements to the system can increase postselection probability while keeping the amplification factor of the weak value A_w unchanged. Such nontrivial improvements scale quadratically with the number of entangled single systems. In our work, we experimentally demonstrate that using even two entangled single systems can make a notable improvement.

Corresponding to our experimental proposal, we designate the identical single-system observable $\hat{a} = \hat{\sigma}_z$ and use two entangled single systems. In addition, the prepared joint state and postselected joint state are $|\psi_i\rangle = \frac{1}{\sqrt{2}}(|00\rangle + |11\rangle)$ and $|\psi_f\rangle \propto -(1 + 2\epsilon)|00\rangle + (1 - 2\epsilon)|11\rangle$, respectively. [This postselected state is different from the corresponding state shown in Fig. 4 of [43], where the postselected state is $|\psi_f\rangle = \frac{1}{\sqrt{2}}(e^{-i\epsilon}|0\rangle^{\otimes n} - e^{i\epsilon}|1\rangle^{\otimes n})$, but that doesn't violate the principle because our choosing of the postselected state fits the form of Eq. (3)] In this case, we can easily derive the weak value of $A_w = 1/\epsilon$ and approximate probability $P_s \approx |\langle \psi_f | \psi_i \rangle|^2 \approx 4\epsilon^2$, which is approximately four times that of the case of no entanglement. Furthermore, we set a series of discrete parameters ϵ for the uncorrelated and correlated cases to keep the amplification factor of the weak value A_w the same, and compare their postselection probabilities. More contrasts are shown in Table I, which clearly verify that adding quantum entanglement can improve weak-value amplification efficiency.

TABLE I. Contrasts of uncorrelated and correlated cases.

	Uncorrelated case	Correlated case
$ \psi_i\rangle$	$ 0\rangle + 1\rangle$	$ 00\rangle + 11\rangle$
$ \psi_f\rangle$	$(1 + \epsilon) 0\rangle - (1 - \epsilon) 1\rangle$	$(1 + 2\epsilon) 00\rangle - (1 - 2\epsilon) 11\rangle$
\hat{A}	$ 0\rangle\langle 0 - 1\rangle\langle 1 $	$I \otimes (0\rangle\langle 0 - 1\rangle\langle 1) + (0\rangle\langle 0 - 1\rangle\langle 1) \otimes I$
$A_w = \langle \psi_f \hat{A} \psi_i \rangle / \langle \psi_f \psi_i \rangle$	$1/\epsilon$	$1/\epsilon$
$P_s \approx \langle \psi_f \psi_i \rangle ^2$	ϵ^2	$4\epsilon^2$

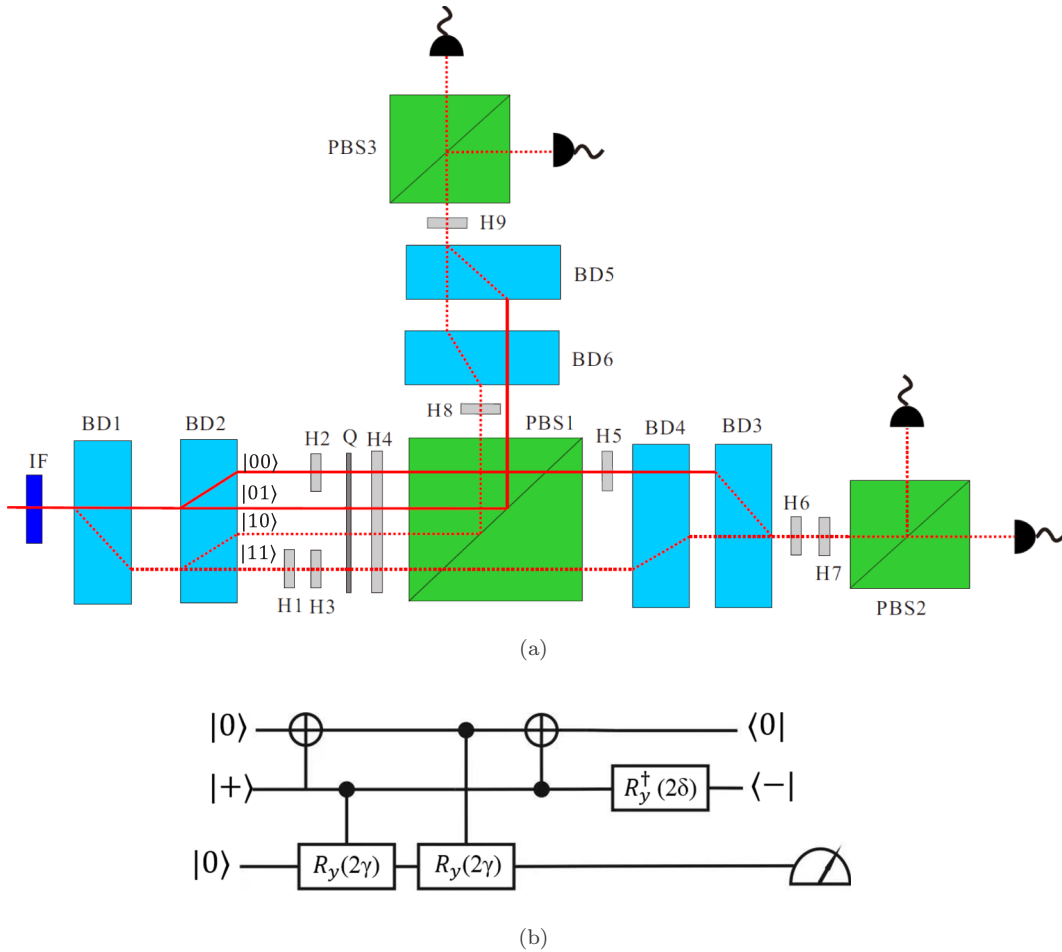


FIG. 1. (a) Experimental setup in correlated case. IF denotes interference filter, BD denotes beam displacer, H denotes half-wave plate, Q denotes quarter-wave plate, and PBS denotes polarizing beam splitter. The single photons, which are produced by generating a pair of photons via spontaneous parametric down conversion (SPDC) with idler photons used as triggers, are prepared into the initial state $|\psi_i\rangle = (|H\rangle + |V\rangle)/\sqrt{2}$ and sent to BD1. Imagine that we look at this setup from the top down; the solid lines represent the upper paths while the dashed lines represent the lower paths. After weak interaction and measurements on the meter observables are performed, postselection and coincidence counting are performed subsequently. H1, H5, H8 are rotated at $\pi/4$, H2 is rotated at 1° , while H3 is rotated at -1° . Q and H4 combining PBS1 after them are used to make projective measurements on the pointer. (b) The corresponding quantum circuit for realizing weak measurements.

III. EXPERIMENTAL REALIZATION OF WEAK-VALUE AMPLIFICATION

A schematic of the weak-value amplification experiment for the correlated case is shown in Fig. 1(a), and the quantum circuit in Fig. 1(b), which simulates the entanglement-assisted weak-value amplification of a small parameter γ , can be compared with that in the theoretical scheme [43]. The meter observables adopted in [43] is the Pauli Z operator $\hat{\sigma}_z$ while in our work we adopt the Pauli Y operator $\hat{\sigma}_y$. The meter qubit is prepared in the state $|0\rangle$, while two coupled single systems are prepared in an entangled state $|\psi_i\rangle$. Each single system is then used as a control for a Y rotation $R_y(2\gamma)$ of the meter, simulating the unitary $U = e^{\gamma \hat{A} \otimes \hat{\sigma}_y/2}$, \hat{A} being the sum of single system observables $\hat{\sigma}_z$ and we use the natural unit such that $\hbar \equiv 1$ in this paper. The entangled state of two coupled single systems is then postselected in an entangled state $|\psi_f\rangle$, and the meter qubit is measured in the eigenstates of pointer observables $\hat{\sigma}_+$ and $\hat{\sigma}_R$, yielding the response relation (6),

which is related to the amplified factor of the weak value A_w . The rotation $R_y(2\delta)$ is used to transform state $\frac{1}{\sqrt{2}}(|0\rangle - |1\rangle)$ to state $(1 + 2\epsilon)|0\rangle - (1 - 2\epsilon)|1\rangle$. The relation between the δ and the ϵ is $\delta = \arctan(2\epsilon)$ (the deduction can be found in Appendix A).

The source of single photons is realized by heralding the coincidence of pairs of photons. Pairs of photons are generated via a spontaneous parametric down-conversion (SPDC) process by pumping a 1-cm-long type-II degenerate PPKTP crystal with a 404-nm continuous-wave laser, the power of which is approximately 15.9 mW. The maximum coincidence counting rate is about 5.3×10^3 per second, and the duration of integration to record the coincidences in our measurement is 30 s. After coupling to a single-mode fiber (SMF), the idler photons are directly sent to a silicon single-photon avalanche detector (SPD) while the signal photons are connected to a launcher and then emitted along the free-space path. The quantum efficiency of the single photon detectors at 808 nm

is about 65%. The extinction ratios of the beam displacers is about 100 000 : 1, and for the polarizing beam splitters is about 10^3 : 1. We used an interference filter (IF; the central wavelength is 808 nm and the bandwidth is 3 nm) before BD1. The signal photons are prepared into the initial state $|\psi_i\rangle = (|H\rangle + |V\rangle)/\sqrt{2}$ by using a polarizing beam splitter (PBS) and a half-wave plate (HWP) after the PBS. The signal photons, after initial-state preparation, are sent to a beam displacer (BD1) for the single-photon state evolution. The beam displacers BD1, BD3, and BD5 are placed in such a way that the vertically polarized (V) component is refracted in the vertical plane while the horizontally polarized (H) component is transmitted directly. BD2, BD4, and BD6 are placed in such a way that the horizontally polarized (H) component is refracted in the horizontal plane while the vertically polarized (V) component is transmitted directly.

The meter and system qubits are encoded on the polarization and path modes of a single photon respectively. We designate horizontal and vertical polarization states as the computational basis $\{|H\rangle, |V\rangle\}$ for the polarization qubit. When photons are sent to BD1, they are split into two paths, in which the V component is shifted down while the H component is transmitted directly. When the photons are sent to BD2, the V component is transmitted directly which is labeled as |down, left), while the H component is shifted laterally right which is labeled as |up, right). Considering the extinction ratio for beam displacers, there are two very weak light beams which are labeled as |down, right) and |up, left). For the path qubit, we designate up (right) and down (left) path modes as the computational basis $\{|0\rangle, |1\rangle\}$, i.e., |up (right) \equiv |0), |down (left) \equiv |1). Specifically, the path coding is shown in the schematic of Fig. 1(a), i.e., |00), |01), |10), and |11) correspond to the path modes of |up, right), |up, right), |up, left), |down, right), and |down, left), respectively.

For weak-value amplification of the correlated case, we designate \hat{A} as follows:

$$\begin{aligned}\hat{A} &\equiv (|\text{up}\rangle\langle\text{up}| - |\text{down}\rangle\langle\text{down}|) \otimes I \\ &\quad + I \otimes (|\text{right}\rangle\langle\text{right}| - |\text{left}\rangle\langle\text{left}|) \\ &\equiv (|0\rangle\langle 0| - |1\rangle\langle 1|) \otimes I + I \otimes (|0\rangle\langle 0| - |1\rangle\langle 1|).\end{aligned}\quad (4)$$

We couple the entangled joint system to the meter according to the interaction Hamiltonian

$$\hat{H}_{\text{int}} = \gamma \hat{A} \otimes \hat{\sigma}_y \delta(t - t_0)/2, \quad (5)$$

which is the key of our setup to perform weak measurement. This weak interaction is implemented with two beam displacers (BD1 and BD2) and several wave plates, which are set as follows: H1 is rotated at $\pi/4$, H2 at $\gamma/2$, and H3 at $-\gamma/2$. The parameter γ , which represents the strength of the coupling interaction, can be continuously adjusted within the accuracy of the experiment. We can couple the entangled joint system to the meter based on the fact that different eigenstates of observable \hat{A} cause different rotations of the pointer depending on the eigenvalue of \hat{A} and the coupling strength γ . For convenience, here we define $|\varphi\rangle \equiv \cos\varphi|H\rangle + \sin\varphi|V\rangle$. Supposing that photons prepared in the polarization state $\alpha|H\rangle + \beta|V\rangle$ are sent into BD1, and after weak interaction, the composite state of photons becomes $\alpha|00\rangle \otimes |\gamma\rangle + \beta|11\rangle \otimes |-\gamma\rangle$, which is

the same state as that of the interaction Hamiltonian \hat{H}_{int} acting on the initial composite state $(\alpha|00\rangle + \beta|11\rangle) \otimes |H\rangle$. Therefore, our experimental setup can realize the interaction Hamiltonian \hat{H}_{int} entirely. We can see that we use the entanglement of two path qubits instead of entanglement of two photons, and there is no nonlocality for the entanglement.

We perform measurements on the meter observables via a quarter-wave plate Q, half-wave plate H4, and polarizing beam splitter PBS1. The reason to do this is that the postselection of the entangled joint system state causes the meter state to rotate at some angle relative to φA_w , so that A_w can be extracted by measuring the conjugate observables of the meter. A_w can be solved from the equations of the expectation value of pointer observables $\hat{\sigma}_+$ and $\hat{\sigma}_R$. Specifically, we have

$$\begin{aligned}\langle\hat{\sigma}_+\rangle &= \frac{1}{2}\text{Re}(A_w) \sin 2\gamma / (\cos^2 \gamma + \frac{1}{4}|A_w|^2 \sin^2 \gamma), \\ \langle\hat{\sigma}_R\rangle &= \frac{1}{2}\text{Im}(A_w) \sin 2\gamma / (\cos^2 \gamma + \frac{1}{4}|A_w|^2 \sin^2 \gamma),\end{aligned}\quad (6)$$

where $\hat{\sigma}_+ = |+\rangle\langle +| - |-\rangle\langle -|$, $\hat{\sigma}_R = |R\rangle\langle R| - |L\rangle\langle L|$, and $|\pm\rangle = (|0\rangle \pm |1\rangle)/\sqrt{2}$, $|R\rangle = (|0\rangle + i|1\rangle)/\sqrt{2}$, $|L\rangle = (|0\rangle - i|1\rangle)/\sqrt{2}$ (more details appear in Appendix B). Such exact expressions establish the condition that the joint system states are superposition states of the orthogonal basis $|00\rangle$ and $|11\rangle$. Our setup can naturally satisfy that condition.

After measurements on meter observables, we postselect the joint system states encoded in path information. The core of our method is to transform the path information into the polarization information. Specifically, we recombine light of both $|00\rangle$ (|up, right) and $|11\rangle$ (|down, left) modes via H5 rotated at $\pi/4$ and two BDs (BD3 and BD4). Note that H1 and H5 transfer the polarization states of the corresponding paths to their opposite polarization states. Therefore, we rotate H6 at $\pi/4$ to recover the state correctly, i.e., if we postselect the polarization state to $|\psi\rangle = \alpha|H\rangle + \beta|V\rangle$, this operation is equal to postselecting the joint state of system to the path mode state $|\psi_f\rangle = \alpha|00\rangle + \beta|11\rangle$.

For a weak-value amplification, we should set a postselection state nearly orthogonal to the initial system state $|\psi_i\rangle = \frac{1}{\sqrt{2}}(|00\rangle + |11\rangle)$. Note that in our experimental proposal we postselect the system into state $|\psi_f\rangle \propto -(1 + 2\epsilon)|00\rangle + (1 - 2\epsilon)|11\rangle$, which is orthogonal to the following basis states:

$$\begin{aligned}|\psi_f^\perp\rangle_0 &\propto (1 - 2\epsilon)|00\rangle + (1 + 2\epsilon)|11\rangle, \\ |\psi_f^\perp\rangle_1 &= |01\rangle, \\ |\psi_f^\perp\rangle_2 &= |10\rangle,\end{aligned}\quad (7)$$

where $|\psi_f^\perp\rangle_0$ is in the state space spanned by $\{|00\rangle, |11\rangle\}$ and is the only state which is orthogonal to $|\psi_f\rangle$ in this space. To measure the probability that we postselect the system into state $|\psi_f\rangle$, we choose our measuring basis as $\{|\psi_f\rangle, |\psi_f^\perp\rangle_0, |\psi_f^\perp\rangle_1, |\psi_f^\perp\rangle_2\}$. In the experiment, we detect coincidence not only for basis $\{|\psi_f\rangle, |\psi_f^\perp\rangle_0\}$ with detectors in the transmission channel of PBS1, but also for basis $\{|\psi_f^\perp\rangle_1, |\psi_f^\perp\rangle_2\}$ with detectors in the reflection channel of PBS1.

To make a direct comparison with the uncorrelated case, we also realize weak measurements for the observable \hat{a} of a single system. The experimental setup of the weak-value amplification measurement for observable \hat{A} is described

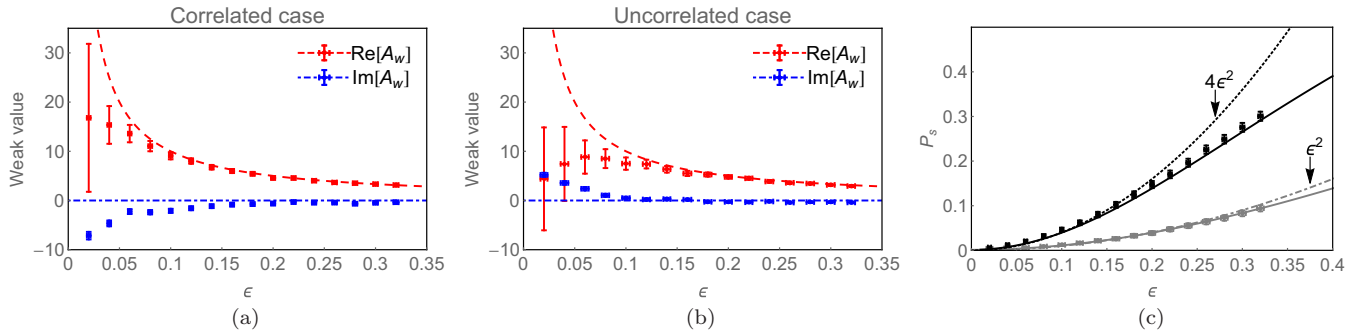


FIG. 2. Experimental results. Correlated and uncorrelated cases are compared using weak values in (a) and (b). For every ϵ , the weak values of the two cases are set to be the same in theory. In (c), we compare the postselection probability of the two different cases in the experiment. Black and gray points correspond to the probability of correlated and uncorrelated cases, black and gray lines correspond to the exact probability of correlated and uncorrelated cases, and black dashed line and gray dotted-dashed line correspond to the approximate probability of correlated and uncorrelated cases. Error bars for (a)–(c) are evaluated on the basis of statistical and system errors, and the statistical errors are evaluated on the basis of Poissonian counting statistics. Here, we consider that system errors are mainly caused by various wave-plate errors, and every wave plate has an alignment error of 0.2° . For the system errors, we calculate them by use of error transfer formula. The wave-plate alignment error results in an error for ϵ ; as a result, there are error bars in the horizontal direction for each data point. (The quantities which we study, such as the ϵ , the weak value, and the probability, are dimensionless, so we have not used units in the above figures.)

in Appendix C. Here, we designate \hat{A} as $\hat{A} \equiv |\text{up}\rangle\langle\text{up}| - |\text{down}\rangle\langle\text{down}| \equiv |0\rangle\langle 0| - |1\rangle\langle 1|$. The interaction Hamiltonian of this uncorrelated case is $\hat{H}_{\text{int}} = \gamma \hat{A} \otimes \hat{\sigma}_y \delta(t - t_0)$. The setting of meter and its coding scheme are the same as mentioned above. The principles and procedures of measurement in the uncorrelated case are analogous to the aforementioned correlated case, and so we will not explore it here (more details can be found in Appendix C).

IV. RESULTS

In our experiment, we perform the weak measurement with $\hat{A} = |0\rangle\langle 0| - |1\rangle\langle 1|$ for the uncorrelated case and $\hat{A} = (|0\rangle\langle 0| - |1\rangle\langle 1|) \otimes I + I \otimes (|0\rangle\langle 0| - |1\rangle\langle 1|)$ for the correlated case such that the weak values of the two observables can be obtained. The parameter γ , which determines measurement strength, is taken with a value of $\gamma = 2^\circ$ for the two cases. We postselect the single system into state $(1 + \epsilon)|0\rangle - (1 - \epsilon)|1\rangle$ (unnormalized) for the uncorrelated case and $(1 + 2\epsilon)|00\rangle - (1 - 2\epsilon)|11\rangle$ (unnormalized) for the correlated case, so for every ϵ , the weak values of the two cases are the same in theory, and we compare them in experiment result. For $\epsilon < 0.1$, the postselected states are nearly orthogonal to the initial state for both cases, so the weak values of both observables are far beyond the observables spectrum. In Figs. 2(a) and 2(b), the theoretical predictions are represented by the red dashed line (real part of A_w) and blue dotted-dashed line (imaginary part of A_w). It can be seen that, for $\epsilon \geq 0.1$, our results fit well with theoretical predictions. For $\epsilon < 0.1$, the results of the experimental measurement show a large deviation from the theoretical predictions, but we deem it reasonable for the following reasons: (1) In our setup and the single-photon system, when ϵ is very small, the rates of single-photon counts will be very low and so our results will be susceptible to the low rates of dark counts and the small difference in the rates of different meter states; and (2) the systematic factors, such as imperfections of polarization extinction of optical elements

and the wave-plate errors, contribute to the degradation of the weak value significantly for small ϵ .

After comparing the weak values for every ϵ in two cases, we next contrast their postselection probabilities in Fig. 2(c). We also deduce the exact solution for postselection probability in the two cases (the deduction can be found in Appendix D), as shown by the black line (correlated case) and gray line (uncorrelated case). It can be seen that when ϵ is small enough (especially for $\epsilon \leq 0.15$ in the uncorrelated case and for $\epsilon \leq 0.3$ in the correlated case), the approximate probability, which has been shown in Table I, fits the exact solution of probability well, but for the rest of the values of ϵ , considerable variation exists between the approximate and exact solutions. Moreover, the larger ϵ is, the larger the variation. This is because the approximation is the first-order approximation of the exact postselection probability and should therefore deviate at larger ϵ . Considering the system errors from imperfections of optical elements, our postselection probability results are in good agreement with theoretical predictions.

V. DISCUSSION AND CONCLUSIONS

We have proposed a concrete experimental scheme for the realization of entanglement-assisted weak-value amplification, and demonstrated it experimentally. We have shown that by introducing quantum entanglement, the postselection probability can be improved effectively compared to the case of no entanglement. The enhancement in postselection efficiency by using entanglement partly offsets the shortcoming of low efficiency in weak-value amplification technology. Furthermore, our scheme and concise experimental setup may provide an intuitive physical picture by which to comprehend the essence of entanglement-assisted weak-value amplification. The theoretical scheme [43] that we have experimentally demonstrated has proposed an improvement that using entanglement can increase the efficiency of weak-value amplification. Our work shows that, to increase the efficiency, one can

use entanglement in system variables, and not necessarily the entanglement of multiple particles and nonlocality. Our work as presented here proves the more extensive application of weak-value amplification, and would promote wider and more profound studies in quantum measurement and metrological techniques [44]. This method can be extended to other experimental systems, such as atomic systems, to measure magnetic fields.

ACKNOWLEDGMENTS

This work was supported by the National Key Research and Development Program of China (Grant No. 2017YFA0304100), NSFC (Grants No. 11874345, No. 11821404, No. 11774335, No. 11734015, No. 11504253, No. 11674306, and No. 61590932), the Key Research Program of Frontier Sciences, CAS (Grant No. QYZDY-SSW-SLH003), the Fundamental Research Funds for the Central Universities, and Anhui Initiative in Quantum Information Technologies (Grants No. AHY020100 and No. AHY060300).

APPENDIX A: RELATION BETWEEN δ AND ϵ

The rotation $R_y(2\delta)$ can be expressed as

$$R_y(2\delta) = \begin{bmatrix} \cos \delta & -\sin \delta \\ \sin \delta & \cos \delta \end{bmatrix}. \quad (\text{A1})$$

After the rotation operator $R_y^\dagger(2\delta)$ function on state $|\psi\rangle = \frac{1}{\sqrt{2}}(|0\rangle - |1\rangle)$, the state $|\psi'\rangle$ will become

$$\begin{aligned} |\psi'\rangle &= R_y(2\delta)|\psi\rangle = \begin{bmatrix} \cos \delta & -\sin \delta \\ \sin \delta & \cos \delta \end{bmatrix} \frac{1}{\sqrt{2}} \begin{pmatrix} 1 \\ -1 \end{pmatrix} \\ &= \frac{1}{\sqrt{2}} \begin{pmatrix} \cos \delta + \sin \delta \\ \sin \delta - \cos \delta \end{pmatrix}. \end{aligned} \quad (\text{A2})$$

$|\psi'\rangle$ is corresponding to our postselection state $(1 + 2\epsilon)|0\rangle - (1 - 2\epsilon)|1\rangle$, and it is requested that

$$\frac{\cos \delta + \sin \delta}{\sin \delta - \cos \delta} = \frac{1 + 2\epsilon}{-(1 - 2\epsilon)}. \quad (\text{A3})$$

The calculation result of the relation between the δ and the ϵ can be expressed as

$$\delta = \arctan(2\epsilon). \quad (\text{A4})$$

APPENDIX B: WEAK VALUE OF OBSERVABLE \hat{A}

We now deduce Eq. (6) in the main text, which shows the relationship between the weak value and the expectation value of pointer observables in the correlated case. In the main text, we designate \hat{A} as $\hat{A} \equiv (|0\rangle\langle 0| - |1\rangle\langle 1|) \otimes I + I \otimes (|0\rangle\langle 0| - |1\rangle\langle 1|)$. So $\hat{A}|0, 0\rangle = 2|0, 0\rangle$, $\hat{A}|0, 1\rangle = 0$, $\hat{A}|1, 0\rangle = 0$, $\hat{A}|1, 1\rangle = -2|1, 1\rangle$. We consider the case in which the initial system states are superposition states of the orthogonal basis $|0, 0\rangle$ and $|0, 1\rangle$, i.e., $|\psi_i\rangle = \alpha|0, 0\rangle + \beta|1, 1\rangle$. We deduce Eq. (6) from the following Taylor expansion:

$$\begin{aligned} e^{-i\hat{A} \otimes \varphi \hat{\sigma}_y} &= I + (-i\hat{A} \otimes \varphi \hat{\sigma}_y) + \frac{1}{2!}(-i\hat{A} \otimes \varphi \hat{\sigma}_y)^2 \\ &\quad + \frac{1}{3!}(-i\hat{A} \otimes \varphi \hat{\sigma}_y)^3 + \dots \\ &\quad + \frac{1}{n!}(-i\hat{A} \otimes \varphi \hat{\sigma}_y)^n + \dots, \end{aligned} \quad (\text{B1})$$

where I is an identity operator. After interaction between the system and pointer, whose effect can be described as a unitary evolution, the state $|\Psi_T\rangle$ of the composite system becomes

$$\begin{aligned} |\Psi_T\rangle &= e^{-i\hat{A} \otimes \varphi \hat{\sigma}_y} |\psi_i\rangle |0\rangle_p \\ &= [I - i\hat{A} \otimes \varphi \hat{\sigma}_y + \frac{(-i\hat{A} \otimes \varphi \hat{\sigma}_y)^2}{2!} + \frac{(-i\hat{A} \otimes \varphi \hat{\sigma}_y)^3}{3!} + \dots + \frac{(-i\hat{A} \otimes \varphi \hat{\sigma}_y)^n}{n!} + \dots] (\alpha|0, 0\rangle + \beta|1, 1\rangle) |0\rangle_p \\ &= \alpha [I + (-i2\varphi \hat{\sigma}_y) + \frac{1}{2!}(-i2\varphi \hat{\sigma}_y)^2 + \frac{1}{3!}(-i2\varphi \hat{\sigma}_y)^3 + \dots + \frac{1}{n!}(-i2\varphi \hat{\sigma}_y)^n + \dots] |0, 0\rangle |0\rangle_p \\ &\quad + \beta [I + (2i\varphi \hat{\sigma}_y) + \frac{1}{2!}(2i\varphi \hat{\sigma}_y)^2 + \frac{1}{3!}(2i\varphi \hat{\sigma}_y)^3 + \dots + \frac{1}{n!}(2i\varphi \hat{\sigma}_y)^n + \dots] |1, 1\rangle |0\rangle_p. \end{aligned} \quad (\text{B2})$$

Using $(\hat{\sigma}_y)^2 = I$, we have

$$\begin{aligned} e^{-i\hat{A} \otimes \varphi \hat{\sigma}_y} |\psi_i\rangle |0\rangle_p &= \alpha \left(I + (-i2\varphi \hat{\sigma}_y) + \frac{1}{2!}(-i2\varphi)^2 + \frac{1}{3!}(-i2\varphi)^3 \hat{\sigma}_y + \dots + \frac{1}{(2k)!}(-i2\varphi)^{2k} + \frac{1}{(2k+1)!}(-i2\varphi)^{2k+1} \hat{\sigma}_y \dots \right) |0, 0\rangle |0\rangle_p \\ &\quad + \beta \left(I + [-i(-2)\varphi \hat{\sigma}_y] + \frac{1}{2!}[-i(-2)\varphi]^2 + \frac{1}{3!}[-i(-2)\varphi]^3 \hat{\sigma}_y + \dots + \frac{1}{(2k)!}[-i(-2)\varphi]^{2k} \right. \\ &\quad \left. + \frac{1}{(2k+1)!}[-i(-2)\varphi]^{2k+1} \hat{\sigma}_y \dots \right) |1, 1\rangle |0\rangle_p. \end{aligned} \quad (\text{B3})$$

We thus have

$$\begin{aligned}
 |\Psi_T\rangle &= \alpha[\cos 2\varphi - i(\sin 2\varphi)\hat{\sigma}_y]|0, 0\rangle|0\rangle_p + \beta[\cos 2\varphi + i(\sin 2\varphi)\hat{\sigma}_y]|1, 1\rangle|0\rangle_p \\
 &= \alpha\left(\cos 2\varphi - i\frac{\hat{A}}{2} \otimes (\sin 2\varphi)\hat{\sigma}_y\right)|0, 0\rangle|0\rangle_p + \beta\left(\cos 2\varphi + i\frac{\hat{A}}{2} \otimes (\sin 2\varphi)\hat{\sigma}_y\right)|1, 1\rangle|0\rangle_p \\
 &= \left(\cos 2\varphi - i\frac{\hat{A}}{2} \otimes (\sin 2\varphi)\hat{\sigma}_y\right)|\psi_i\rangle|0\rangle_p. \tag{B4}
 \end{aligned}$$

The state of the pointer, after the system is postselected into state $|\psi_f\rangle$, becomes (unnormalized)

$$\begin{aligned}
 |\tilde{\varphi}_p\rangle &= \langle\psi_f|\Psi_T\rangle \\
 &= \langle\psi_f|\left(\cos 2\varphi - i\frac{\hat{A}}{2} \otimes \sin 2\varphi\hat{\sigma}_y\right)|\psi_i\rangle|0\rangle_p \\
 &= \left(\cos 2\varphi\langle\psi_f|\psi_i\rangle - i\sin 2\varphi\langle\psi_f|\frac{\hat{A}}{2}|\psi_i\rangle\hat{\sigma}_y\right)|0\rangle_p. \tag{B5}
 \end{aligned}$$

Using the definitions of $\langle\hat{A}\rangle_w = \langle\psi_f|\hat{A}|\psi_i\rangle/\langle\psi_f|\psi_i\rangle$ and $i\hat{\sigma}_y = |0\rangle_p\langle 1|_p - |1\rangle_p\langle 0|_p$, we obtain

$$\begin{aligned}
 |\tilde{\varphi}_p\rangle &= [(\cos 2\varphi\langle\psi_f|\psi_i\rangle - i\sin 2\varphi A_w\langle\psi_f|\psi_i\rangle\hat{\sigma}_y/2)|0\rangle_p] \\
 &= [\cos 2\varphi\langle\psi_f|\psi_i\rangle|0\rangle_p + \sin 2\varphi A_w\langle\psi_f|\psi_i\rangle/2|1\rangle_p]. \tag{B6}
 \end{aligned}$$

The norm of $|\tilde{\varphi}_p\rangle$ is

$$\sqrt{|\langle\tilde{\varphi}_p|\tilde{\varphi}_p\rangle|} = |\langle\psi_f|\psi_i\rangle|\sqrt{(\cos^2 2\varphi + \frac{1}{4}|A_w|^2 \sin^2 2\varphi)}. \tag{B7}$$

In our representation, $\hat{\sigma}_+ = \begin{bmatrix} 0 & 1 \\ 1 & 0 \end{bmatrix}$, $\hat{\sigma}_R = \begin{bmatrix} 0 & -i \\ i & 0 \end{bmatrix}$, so

$$\begin{aligned}
 \langle\tilde{\varphi}_p|\hat{\sigma}_+|\tilde{\varphi}_p\rangle &= |\langle\psi_f|\psi_i\rangle|^2 (\cos 2\varphi, \frac{1}{2}A_w^* \sin 2\varphi)\hat{\sigma}_+\begin{pmatrix} \cos 2\varphi \\ \frac{1}{2}A_w \sin 2\varphi \end{pmatrix} \\
 &= |\langle\psi_f|\psi_i\rangle|^2 (\cos 2\varphi, \frac{1}{2}A_w^* \sin 2\varphi)\begin{pmatrix} \frac{1}{2}A_w \sin 2\varphi \\ \cos 2\varphi \end{pmatrix} \\
 &= |\langle\psi_f|\psi_i\rangle|^2 \cos 2\varphi \sin 2\varphi (A_w^* + A_w)/2 \\
 &= |\langle\psi_f|\psi_i\rangle|^2 \sin 4\varphi \text{Re}[A_w]/2. \tag{B8}
 \end{aligned}$$

Finally, the expectation value of pointer observable $\hat{\sigma}_+$ is

$$\begin{aligned}
 \langle\hat{\sigma}_+\rangle_p &= \langle\tilde{\varphi}_p|\hat{\sigma}_+|\tilde{\varphi}_p\rangle/\langle\tilde{\varphi}_p|\tilde{\varphi}_p\rangle \\
 &= \frac{1}{2} \sin 4\varphi \text{Re}[A_w]/(\cos^2 2\varphi + \frac{1}{4}|A_w|^2 \sin^2 2\varphi). \tag{B9}
 \end{aligned}$$

By the same method, the expectation value of the pointer observable $\hat{\sigma}_R$ can be deduced as

$$\begin{aligned}
 \langle\hat{\sigma}_R\rangle_p &= \langle\tilde{\varphi}_p|\hat{\sigma}_R|\tilde{\varphi}_p\rangle/\langle\tilde{\varphi}_p|\tilde{\varphi}_p\rangle \\
 &= \frac{1}{2} \sin 4\varphi \text{Im}[A_w]/(\cos^2 2\varphi + \frac{1}{4}|A_w|^2 \sin^2 2\varphi). \tag{B10}
 \end{aligned}$$

In the main text, $\hat{H}_{\text{int}} = \gamma\hat{A} \otimes \hat{\sigma}_y\delta(t - t_0)/2$, so the unitary evolution can be described as

$$U = e^{\gamma\hat{A} \otimes \hat{\sigma}_y/2}, \tag{B11}$$

We set $\varphi = \gamma/2$, and Eq. (6) in the main text can be easily deduced. Above, we deduce the equations for the weak value A_w and the expectation value of pointer observables in the correlated case, from which we can measure A_w by measuring the expectation value of pointer observables $\hat{\sigma}_+$ and $\hat{\sigma}_R$ and then solving the related equations.

We now discuss the analogous equations for the uncorrelated case. In this case, $\hat{H}_{\text{int}} = \varphi\hat{A} \otimes \hat{\sigma}_y\delta(t - t_0)$ and $\hat{A} = \hat{\sigma}_z = |0\rangle\langle 0| - |1\rangle\langle 1|$. One can use similar methods as above to deduce the following equations [6]:

$$\begin{aligned}
 \langle\hat{\sigma}_+\rangle_p &= \langle\tilde{\varphi}_p|\hat{\sigma}_+|\tilde{\varphi}_p\rangle/\langle\tilde{\varphi}_p|\tilde{\varphi}_p\rangle \\
 &= \sin 2\varphi \text{Re}[A_w]/(\cos^2 \varphi + |A_w|^2 \sin^2 \varphi). \tag{B12}
 \end{aligned}$$

$$\begin{aligned}
 \langle\hat{\sigma}_R\rangle_p &= \langle\tilde{\varphi}_p|\hat{\sigma}_R|\tilde{\varphi}_p\rangle/\langle\tilde{\varphi}_p|\tilde{\varphi}_p\rangle \\
 &= \sin 2\varphi \text{Im}[A_w]/(\cos^2 \varphi + |A_w|^2 \sin^2 \varphi). \tag{B13}
 \end{aligned}$$

APPENDIX C: EXPERIMENTAL SETUP FOR REALIZING WEAK MEASUREMENTS IN UNCORRELATED CASE

In Fig. 3, BD1 and BD2 are placed in such a way that the vertically polarized (V) component is refracted in the vertical plane, while the horizontally polarized (H) component is transmitted directly. In this schematic, BD denotes the beam displacer, H is the half-wave plate, Q is the quarter-wave plate, and PBS is the polarizing beam splitter. Path coding is shown in the schematic, i.e., $|0\rangle$ and $|1\rangle$ correspond, respectively, to path modes of $|\text{up}\rangle$ and $|\text{down}\rangle$.

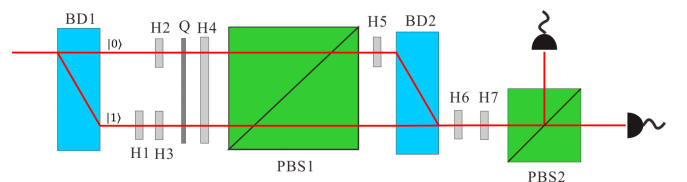


FIG. 3. Experimental setup for realizing weak measurements in the uncorrelated case.

APPENDIX D: DEDUCTION OF POSTSELECTION PROBABILITY IN CURRENT EXPERIMENT

We still first deduce the postselection probability for the correlated case. From Eq. (A3), we deduce that

$$\begin{aligned} |\Psi_T\rangle &= \alpha(\cos 2\varphi|0\rangle_p + (\sin 2\varphi)|1\rangle_p)|0, 0\rangle \\ &\quad + \beta(\cos 2\varphi|0\rangle_p - \sin 2\varphi|1\rangle_p)|1, 1\rangle \\ &= \alpha|2\varphi\rangle|0, 0\rangle + \beta|-2\varphi\rangle|1, 1\rangle. \end{aligned} \quad (\text{D1})$$

Then, the state of the pointer, after the system is postselected into state $|\psi_f\rangle$, becomes (unnormalized)

$$|\tilde{\varphi}_p\rangle = \langle\psi_f|\Psi_T\rangle. \quad (\text{D2})$$

In our experiment, $|\psi_f\rangle = (1 + 2\epsilon)|0, 0\rangle - (1 - 2\epsilon)|1, 1\rangle$ (unnormalized), $|\psi_f^\perp\rangle = (1 - 2\epsilon)|0, 0\rangle + (1 + 2\epsilon)|1, 1\rangle$, and $|\psi_i\rangle = |0, 0\rangle + |1, 1\rangle$ (unnormalized), so

$$\begin{aligned} |\tilde{\varphi}_p\rangle &= \langle\psi_f|\Psi_T\rangle \\ &= [(1 + 2\epsilon)\langle 0, 0| - (1 - 2\epsilon)\langle 1, 1|]\Psi_T \\ &= [(1 + 2\epsilon)\langle 0, 0| - (1 - 2\epsilon)\langle 1, 1|][|2\varphi\rangle|0, 0\rangle + |-2\varphi\rangle|1, 1\rangle] \\ &= (1 + 2\epsilon)|2\varphi\rangle - (1 - 2\epsilon)|-2\varphi\rangle, \end{aligned} \quad (\text{D3})$$

and by the same method, we have

$$\begin{aligned} |\tilde{\varphi}_p^\perp\rangle &= \langle\psi_f^\perp|\Psi_T\rangle \\ &= (1 - 2\epsilon)|2\varphi\rangle + (1 + 2\epsilon)|-2\varphi\rangle. \end{aligned} \quad (\text{D4})$$

Note that we perform measurements on the meter observables $\hat{\sigma}_+$ using bases $|+\rangle_p$ and $|-\rangle_p$, so the postselection probability is calculated as follows:

$$P = \frac{N_0}{N_0 + N_1}, \quad (\text{D5})$$

while $N_0 = |\langle +|\tilde{\varphi}_p\rangle|^2 + |\langle -|\tilde{\varphi}_p\rangle|^2$ and $N_1 = |\langle +|\tilde{\varphi}_p^\perp\rangle|^2 + |\langle -|\tilde{\varphi}_p^\perp\rangle|^2$. We further deduce that

$$P = \frac{4\epsilon^2 \cos^2 2\varphi + \sin^2 2\varphi}{1 + 4\epsilon^2}. \quad (\text{D6})$$

By the same method, we deduce that the postselection probability for the uncorrelated case is

$$P = \frac{\epsilon^2 \cos^2 \varphi + \sin^2 \varphi}{1 + \epsilon^2}. \quad (\text{D7})$$

-
- [1] Y. Aharonov, D. Z. Albert, and L. Vaidman, How the Result of a Measurement of a Component of the Spin of a Spin-1/2 Particle Can Turn Out to be 100, *Phys. Rev. Lett.* **60**, 1351 (1988).
- [2] G. J. Pryde, J. L. O'Brien, A. G. White, T. C. Ralph, and H. M. Wiseman, Measurement of Quantum Weak Values of Photon Polarization, *Phys. Rev. Lett.* **94**, 220405 (2005).
- [3] G. Mitchison, R. Jozsa, and S. Popescu, Sequential weak measurement, *Phys. Rev. A* **76**, 062105 (2007).
- [4] F. Piacentini, A. Avella, M. P. Levi, M. Gramegna, G. Brida, and I. P. Degiovanni, Measuring Incompatible Observables by Exploiting Sequential Weak Values, *Phys. Rev. Lett.* **117**, 170402 (2016).
- [5] Y. Kim, Y. S. Kim, S. Y. Lee, S. W. Han, S. Moon, Y. H. Kim, and Y. W. Cho, Direct quantum process tomography via measuring sequential weak values of incompatible observables, *Nat. Commun.* **9**, 192 (2018).
- [6] J. S. Chen, M. J. Hu, X. M. Hu, B. H. Liu, Y. F. Huang, C. F. Li, G. C. Guoy, and Y. S. Zhang, Experimental realization of sequential weak measurements of non-commuting Pauli observables, *Opt. Express* **27**, 6089 (2019).
- [7] M. Pusey, Anomalous Weak Values are Proofs of Contextuality, *Phys. Rev. Lett.* **113**, 200401 (2014).
- [8] F. Piacentini, A. Avella, M. P. Levi, R. Lussana, F. Villa, A. Tosi, F. Zappa, M. Gramegna, G. Brida, I. P. Degiovanni, and M. Genovese, Experiment Investigating the Connection Between Weak Values and Contextuality, *Phys. Rev. Lett.* **116**, 180401 (2016).
- [9] K. J. Resch, K. J. Lundeen, and A. M. Steinberg, Experimental realization of the quantum box problem, *Phys. Lett. A* **324**, 125 (2004).
- [10] J. S. Lundeen and A. M. Steinberg, Experimental Joint Weak Measurement on a Photon Pair as a Probe of Hardy's Paradox, *Phys. Rev. Lett.* **102**, 020404 (2009).
- [11] K. Yokota, T. Yamamoto, M. Koashi, and N. Imoto, Direct observation of Hardy's paradox by joint weak measurement with an entangled photon pair, *New J. Phys.* **11**, 033011 (2009).
- [12] Y. Aharonov, A. Botero, S. Popescu, B. Reznik, and J. Tollaksen, Revisiting Hardy's Paradox: counterfactual statements, real measurements, entanglements and weak values, *Phys. Lett. A* **301**, 130 (2002).
- [13] N. S. Williams and A. N. Jordan, Weak Values and the Leggett-Garg Inequality in Solid-State Qubits, *Phys. Rev. Lett.* **100**, 026804 (2008).
- [14] J. Z. Salvail, M. Agnew, A. S. Johnson, E. Bolduc, J. Leach, and R. W. Boyd, Full characterization of polarization states of light via direct measurement, *Nat. Photon.* **7**, 316 (2013).
- [15] J. S. Lundeen, B. Sutherland, A. Patel, C. Stewart, and C. Bamber, Direct measurement of the quantum wavefunction, *Nature (London)* **474**, 188 (2011).
- [16] M. Malik, M. Mirhosseini, M. P. J. Lavery, J. Leach, M. J. Padgett, and R. W. Boyd, Direct measurement of a 27-dimensional orbital-angular-momentum state vector, *Nat. Commun.* **5**, 3115 (2014).
- [17] J. S. Lundeen and C. Bamber, Procedure for Direct Measurement of General Quantum States Using Weak Measurements, *Phys. Rev. Lett.* **108**, 070402 (2012).
- [18] L. Hardy, Quantum Mechanics, Local Realistic Theories, and Lorentz-Invariant Realistic Theories, *Phys. Rev. Lett.* **68**, 2981 (1992).
- [19] Y. Aharonov and L. Vaidman, *Time in Quantum Mechanics* (Springer, New York, 2002), pp. 369–412.
- [20] A. G. Kofman, S. Ashhab, and F. Nori, Nonperturbative theory of weak pre- and post-selected measurements, *Phys. Rep.* **520**, 43 (2012).
- [21] J. Dressel, M. Malik, F. M. Miatto, A. N. Jordan, and R. W. Boyd, Understanding quantum weak values: basics and applications, *Rev. Mod. Phys.* **86**, 307 (2014).

- [22] O. Hosten and P. Kwiat, Observation of the spin Hall effect of light via weak measurements, *Science* **319**, 787 (2008).
- [23] K. J. Resch, Amplifying a tiny optical effect, *Science* **319**, 733 (2008).
- [24] P. B. Dixon, D. J. Starling, A. N. Jordan, and J. C. Howell, Ultrasensitive Beam Detection Measurement Via Interferometric Weak Value Amplification, *Phys. Rev. Lett.* **102**, 173601 (2009).
- [25] A. M. Steinberg, A light touch, *Nature (London)* **463**, 890 (2010).
- [26] N. Brunner and C. Simon, Measuring Small Longitudinal Phase Shifts: Weak Measurements or Standard Interferometry? *Phys. Rev. Lett.* **105**, 010405 (2010).
- [27] A. Feizpour, X. Xing, and A. M. Steinberg, Amplifying Single-Photon Nonlinearity Using Weak Measurements, *Phys. Rev. Lett.* **107**, 133603 (2011).
- [28] M. Hallaji, A. Feizpour, G. Dmochowski, J. Sinclair, and A. M. Steinberg, Weak-value amplification of the nonlinear effect of a single photon, *Nat. Phys.* **13**, 540 (2017).
- [29] G. Strubi and C. Bruder, Measuring Ultrasmall Time Delays of Light by Joint Weak Measurements, *Phys. Rev. Lett.* **110**, 083605 (2013).
- [30] X. Y. Xu, Y. Kedem, K. Sun, L. Vaidman, C. F. Li, and G. C. Guo, Phase Estimation with Weak Measurement Using a White Light Source, *Phys. Rev. Lett.* **111**, 033604 (2013).
- [31] G. C. Knee, G. A. D. Briggs, S. C. Benjamin, and E. M. Gauger, Quantum sensors based on weak-value amplification cannot overcome decoherence, *Phys. Rev. A* **87**, 012115 (2013).
- [32] N. W. M. Ritchie, J. G. Story, and R. G. Hulet, Realization of a Measurement of a “Weak Value”, *Phys. Rev. Lett.* **66**, 1107 (1991).
- [33] X. Zhu, Y. Zhang, S. Pang, C. Qiao, Q. Liu, and S. Wu, Quantum measurements with preselection and postselection, *Phys. Rev. A* **84**, 052111 (2011).
- [34] S. Pang and T. A. Brun, Improving the Precision of Weak Measurements by Postselection Measurement, *Phys. Rev. Lett.* **115**, 120401 (2015).
- [35] G. B. Alves, B. M. Escher, R. L. de Matos Filho, N. Zagury, and L. Davidovich, Weak-value amplification as an optimal metrological protocol, *Phys. Rev. A* **91**, 062107 (2015).
- [36] J. Combes, C. Ferrie, Z. Jiang, and C. M. Caves, Quantum limits on postselected, probabilistic quantum metrology, *Phys. Rev. A* **89**, 052117 (2014).
- [37] C. Ferrie and J. Combes, Weak Value Amplification is Suboptimal for Estimation and Detection, *Phys. Rev. Lett.* **112**, 040406 (2014).
- [38] S. Tanaka and N. Yamamoto, Information amplification via postselection: A parameter-estimation perspective, *Phys. Rev. A* **88**, 042116 (2013).
- [39] G. C. Knee and E. M. Gauger, When Amplification with Weak Values Fails to Suppress Technical Noise, *Phys. Rev. X* **4**, 011032 (2014).
- [40] L. Zhang, A. Datta, and I. A. Walmsley, Precision Metrology Using Weak Measurements, *Phys. Rev. Lett.* **114**, 210801 (2015).
- [41] A. N. Jordan, J. Martínez-Rincón, and J. C. Howell, Technical Advantages for Weak-Value Amplification: When Less is More, *Phys. Rev. X* **4**, 011031 (2014).
- [42] J. Harris, R. W. Boyd, and J. S. Lundeen, Weak Value Amplification Can Outperform Conventional Measurement in the Presence of Detector Saturation, *Phys. Rev. Lett.* **118**, 070802 (2017).
- [43] S. Pang, J. Dressel, and T. A. Brun, Entanglement-Assisted Weak Value Amplification, *Phys. Rev. Lett.* **113**, 030401 (2014).
- [44] V. Giovannetti, S. Lloyd, and L. Maccone, Advances in quantum metrology, *Nat. Photon.* **5**, 222 (2011).